

# Spin dissymmetry in optical cavities.

Jefferson Dixon<sup>1\*</sup>, Zachary N. Mauri<sup>2</sup>, Christopher J. Ciccarino<sup>2</sup>, Priyanuj Bordoloi<sup>2</sup>, Feng Pan<sup>2</sup>,  
Felipe H. da Jornada<sup>2</sup>, Jennifer Dionne<sup>2\*</sup>.

<sup>1</sup> Department of Mechanical Engineering, Stanford University, Stanford, California 94305, USA

<sup>2</sup> Department of Materials Science and Engineering, Stanford University, Stanford, California 94305,  
USA

## Abstract

We introduce the spin dissymmetry factor, a measure of the spin-selectivity in the optical transition rate of quantum particles. This spin dissymmetry factor is valid locally, including at material interfaces and within optical cavities. We design and numerically demonstrate an optical cavity with three-fold rotational symmetry that maximizes spin dissymmetry, thereby minimizing the spin dephasing of a cavity-coupled quantum particle. Our approach emphasizes the difference between spin and chirality in the nearfield and reveals a classical parameter for designing more efficient quantum optical devices.

## Main Text

### Introduction

Spin is a fundamental property of elementary particles, including electrons and photons. From a classical perspective, we observe the spin of light through its polarization, known as circularly polarized light (CPL). The symmetry of circularly polarized light interacts selectively with the intrinsic spin of electrons, establishing the foundation of quantum optics used in materials characterization and optically-addressable spin quantum bits (qubits) (1).

Chirality is a property of objects that cannot be superimposed on their mirror image, such as in chiral molecules (*e.g.*, amino acids, sugars) (2). Circularly polarized light can be referred to as itself chiral, although this definition becomes ambiguous when the wavevector is not uniformly defined (*e.g.*, in the nearfield) (3, 4). The exploration of spin-orbit coupling in classical Maxwell's Equations has given a local description of optical chirality that simultaneously elucidates a close, but distinct, relationship to optical spin (5, 6). The local description of chirality, known as Kuhn's dissymmetry factor, has been foundational to decades of developments in chiral optical cavities, molecular detection, and synthesis (7-9).

Here we present the spin dissymmetry factor, which is a normalized measure of the local confinement of light (*i.e.*, local density of optical states) in a parity-even and time-odd basis. The resulting classical quantity is directly related to the transition rate of a quantum particle, where the magnitude and sign of the spin dissymmetry factor is proportional to the magnitude and phase of spin coherence. We show that the spin dissymmetry factor can be maximized in a metasurface cavity relying on quasi-bound states

in the continuum with at least three-fold rotational symmetry, which is a consequence of the topological distribution of optical currents.

## Results

The relationship between chirality and spin is defined in quantum field theory through the helicity operator,

$$\hat{h} = \hat{\mathbf{S}} \cdot \frac{\mathbf{p}}{p} \quad (1)$$

Where the helicity operator  $\hat{h}$ , is defined as the spin operator  $\hat{\mathbf{S}}$  (equivalent to the Pauli spin matrices multiplied by Planck's constant) projected along the direction of the particle momentum  $\mathbf{p}$  (12, 13). Bold letters indicate vectors, so that helicity  $h$  is a pseudoscalar arising from the three-dimensional space  $\mathbf{S} \otimes \mathbf{p}$  when spin is transverse to the direction of linear momentum. For massless particles such as photons, the chirality of light is identical to this helicity. The parity-odd symmetry of chirality and parity-even symmetry of spin is presented in Table 1; the operators, associated eigenmodes, and interaction polarizabilities follow this same symmetry.

Consider a state vector composed of complex (time-varying) electric and magnetic fields that vary in space  $\mathbf{r}$  such that,

$$\Psi(\mathbf{r}) = \frac{1}{2\sqrt{\omega}} \begin{pmatrix} \mathbf{E}(\mathbf{r}) \\ \mathbf{H}(\mathbf{r}) \end{pmatrix}. \quad (2)$$

Here the units  $c = \epsilon_0 = \mu_0 = 1$  are assumed, and the transversality condition of electric and magnetic fields is ensured by  $\hat{\mathbf{p}} \cdot \Psi(\mathbf{r}) = 0$ , with the momentum operator  $\hat{\mathbf{p}} = -i\nabla$  (14). We can map the electric and magnetic fields from Equation 2 in a spin basis or chiral basis by operating on them with Equation 1. The time-averaged local expectation values of spin and chirality are then, respectively,

$$\mathbf{S} = \langle \Psi | \hat{\mathbf{S}} | \Psi \rangle = \frac{1}{4\omega} \text{Imag}(\mathbf{E}^* \times \mathbf{E} + \mathbf{H}^* \times \mathbf{H}), \quad (3)$$

$$C = \langle \Psi | \hat{h} | \Psi \rangle = -\frac{1}{2\omega} \text{Imag}(\mathbf{E}^* \cdot \mathbf{H}), \quad (4)$$

Where  $\mathbf{S}$  and  $C$  vary spatially as a function of  $\mathbf{r}$ , and the asterisks indicate the complex conjugate. Spin density  $S$  can be defined for a two-dimensional plane, whereas chiral density  $C$  can only be defined for a three-dimensional volume. For completeness, we also evaluate the local electromagnetic energy density,

$$W = \langle \Psi | \omega | \Psi \rangle = \frac{1}{4} (|\mathbf{E}|^2 + |\mathbf{H}|^2). \quad (5)$$

The values for spin density  $\mathbf{S}$ , chiral density  $C$ , and electromagnetic energy density  $W$  are valid locally even when the wavevector is not well defined, such as in the nearfield of subwavelength cavities (see Supporting Information 1).

When electromagnetic fields are confined in an optical cavity, the local density of optical states (LDOS) is modified. The transition rate of quantum particle excited by light (*i.e.*, rate of optical absorption) is proportional to this local density of optical states. This is known as Fermi's Golden Rule, written for an interaction Hamiltonian in the Coulomb gauge ( $\nabla \cdot \mathbf{A} = 0$ ) with the form (15, 16),

$$\hat{\mathcal{H}}^{int} = \frac{e}{m_e c} \mathbf{A}^\pm(\mathbf{r}, t) \cdot \mathbf{p}, \quad (6)$$

Where  $e$  is the charge of an electron,  $m_e$  is the mass of an electron,  $\mathbf{p}$  is the momentum vector, and we have omitted the diamagnetic term proportional to  $A^2$ . The vector potential in this choice of gauge is,

$$\mathbf{A}^\pm(\mathbf{r}, t) = A_0 \hat{\mathbf{e}}^\pm e^{i(\mathbf{q} \cdot \mathbf{r} - \omega t)}, \quad (7)$$

Such that the spatial dependence of the external field is related to the wavevector of the incident light, and the polarization vector  $\hat{\epsilon}^\pm$  determines the handedness of the photon. By restricting our focus to near-field interactions, we consider only the vector potential at a point  $r_0$ , creating a local definition. This simplification yields a result equivalent to that which is obtained from the long wavelength approximation ( $\mathbf{q} \approx 0$ ).

Treating the light-matter interaction as a perturbation to a ground state many-body Hamiltonian, we then apply time-dependent perturbation theory to arrive at (15),

$$\Gamma_{i \rightarrow f}^\pm(\mathbf{k}) = \frac{2\pi e^2 A_0^2}{\hbar c^2 m^2} |\langle f|\mathbf{k}|\hat{\epsilon}^\pm \cdot \mathbf{p}|i\rangle|^2 \delta(E_f(\mathbf{k}) - E_i(\mathbf{k}) - \hbar\omega)(f_i(\mathbf{k}) - f_f(\mathbf{k})), \quad (8)$$

for the transition rate of an electron from the band  $i$  to band  $f$ . We can then obtain a measure of the spin-selectivity of such excitations at each point in the dispersion,

$$\eta_{v \rightarrow c}(\mathbf{k}) = \frac{\text{Imag}[\mathbf{p}_{cv}^*(\mathbf{k}) \times \mathbf{p}_{cv}(\mathbf{k})]}{|\mathbf{p}_{cv}(\mathbf{k})|^2}, \quad (9)$$

Which uses the momentum matrix element of the transition,  $p_{cv}(\mathbf{k})$ . This process underlies the origin of spin-selection rules in a variety of quantum materials, such as the creation of an exciton in a monolayer transition metal dichalcogenide (2D TMDC). More generally, this describes the relative absorption of light into one eigenstate of a Kramers' degenerate pair when time-reversal symmetry is broken.

Finally, we maximize the light-matter interaction Hamiltonian (Equation 6) dot product by aligning the vector potential (Equation 7) with the momentum vector of the transition (Equation 9). This is solved using classical electric fields of the form,

$$\mathbf{s}(\mathbf{r}) = \frac{\text{Imag}(\mathbf{E}(\mathbf{r})^* \times \mathbf{E}(\mathbf{r}))}{|\mathbf{E}(\mathbf{r})_0|^2}, \quad (10)$$

And aligning the quantum particle along the principal coordinate axis as,

$$s = \frac{\text{Imag}(\mathbf{E}_\parallel^* \cdot \mathbf{E}_\perp - \mathbf{E}_\perp^* \cdot \mathbf{E}_\parallel)}{|\mathbf{E}_0|^2}. \quad (11)$$

Equation 11 maximizes optical interaction with a general spin-selective transition in matter, which we refer to as the (local) *spin dissymmetry factor*. This is the fundamental result of this report. The spin dissymmetry factor quantity spans [-1, 1] for monochromatic plane waves, where it is 1, -1 for circularly polarized light and 0 for linearly polarized light. For optical cavities that increase the local density of optical states beyond that of free space, the absolute value exceeds 1.

## Discussion

Like the Kuhn (chiral) dissymmetry factor (which is the normalized chiral energy density), and the Purcell factor (which is the normalized electric energy density), the spin dissymmetry factor has dimensionless units (see Supporting Information 2). This factor can be viewed as the normalized spin energy density or electric spin angular momentum, and it is compared directly to the Kuhn dissymmetry factor and Purcell factor in Table 1. Upon inspection, we see that that primary difference between the spin dissymmetry factor and Kuhn dissymmetry factor is in the separability of their electric and magnetic parts; spin can be viewed in a purely electric basis whereas chirality is always electromagnetic. Spin objects (nonmagnetic) are modeled with the usual electric polarizability while chiral objects are modeled with a (bi)anisotropic polarizability. In other words, the spin dissymmetry factor can only be applied for interactions with matter that preserves mirror symmetry, while the Kuhn dissymmetry factor can only be applied when the interacting matter has broken mirror symmetry.

We explore a model system to illustrate spin dissymmetry in a subwavelength optical cavity. Consider a dielectric metasurface composed of disks arranged in a staggered hexagonal (i.e., honeycomb) lattice (see Methods Section). The difference in diameter of neighboring disks allows an anti-symmetric dark mode (bound state in the continuum, or BIC) to become bright and radiate into the far-field (quasi-bound state in the continuum, or q-BIC) with a high-quality factor (high-q) resonance.

Our high-Q dielectric metasurface is studied as an optical cavity to enhance coupling with a quantum particle possessing out-of-plane spin. We plot the normalized spin dissymmetry and compare it to the normalized Kuhn (chiral) dissymmetry (Fig 1a,b). Dielectric Mie particles, like the disks in our metasurface, exhibit both electric-type and magnetic-type eigenmodes; the electric-type mode that we consider here has in-plane electric field vectors spinning to generate out-of-plane spin. The spin density only requires that the near-field preserves the circular rotation of CPL, which is achieved with a cavity possessing rotational symmetry  $C_n \geq 3$  (17). Chiral density, however, requires co-occurrence of the electric and magnetic fields in addition to their rotation; the asymmetric Fano line shape reflects the interference between electric and magnetic oscillations across the resonance (18). The requirement of  $C_n \geq 3$  rotational symmetry aligned with the axis of propagation is difficult to achieve in on-chip photonics due to the symmetry-breaking of the substrate, making photonic crystals and metasurfaces particularly attractive for spin and chiral optics.

Optical currents of both negative and positive spin occur because of the open topology of the cavity (i.e., net zero topological charge is preserved). However, the rotationally symmetric q-BIC resonances concentrate light selectively over regions of spin with a single sign, such that the spin dissymmetry is maximized. In Figure 1c, we plot the spin density and optical currents (see Supporting Information 3) of the same mode considered in Figure 1a,b. Here, we see that the optical currents circulate about the centers of large spin dissymmetry and avoid centers of low spin dissymmetry. Similarly, the current centers that are located over regions of high (low) energy density correlate with centers of high (low) dissymmetry, and this persists throughout the mode volume. Ultimately, this behavior is a consequence of the preferential distribution of topological charge introduced by the rotationally symmetric q-BIC mode, and we expect this behavior in a variety of high-symmetry lattice configurations.

In conclusion, we introduce the spin dissymmetry factor to quantify local enhancement (i.e., increase in the local density of optical states) in a spin basis, akin to how the Kuhn dissymmetry factor quantifies enhancement in a chiral basis. Like the Purcell factor, the spin dissymmetry factor increases with the cavity quality factor (19). Unlike the Purcell factor, this spin dissymmetry factor simultaneously accounts for both spectral coherence and phase (spin) coherence. We design a high-Q optical cavity that distributes optical currents to maximize the spin dissymmetry, which minimizes the spin dephasing of a coupled particle. This advancement, especially in conjunction with the development of more robust quantum emitters (e.g., 2D TMDCs, Moire superlattices), may help push quantum computing to more practical operating temperatures without sacrificing fidelity. The design principles presented here may also be applied to other spin systems, such as topological objects like skyrmions and anyons, nonlinear and nonreciprocal systems, and quantum measurements.

## Materials and Methods

The numerical calculations for the metasurface are performed using the Electromagnetics Module in COMSOL Multiphysics, which is a commercial Finite Element Analysis solver. The COMSOL model is a 4-port simulation with periodic boundary conditions, where the ports assume Floquet periodicity. We

illuminate the metasurface with circularly polarized light, either right-handed (RCP) or left-handed (LCP). The metasurface is comprised of disks with a refractive index of 3.5 and are lossless.

The dimensions of the metasurface are normalized by the lattice constant  $a$ , where the disk height  $h = a/3$  and the disk diameter  $d = 9a/5$ ; the diffraction limit is at  $D = 3a/2$ . We manipulate the inversion symmetry of the lattice by changing the diameter of neighboring disks ( $\delta > 0$ ), resulting in a high quality-factor (high-Q) resonance in transmission. This high-Q mode is a symmetry-protected quasi-bound state in the continuum (q-BIC), with a resonance linewidth that can be tuned using the difference in disk diameters following the relation  $Q \propto \frac{1}{\delta^2}$  (20).

The calculations for normalized spin dissymmetry  $s$  (Fig 1a) and normalized chiral (Kuhn) dissymmetry  $g$  (Fig 1b) are averaged over the simulation volume from  $z = 0$  to  $z = h$ . Equations 7 and 8 also take the  $E_0$  value for CPL in free space, such that the values for Equations 7 and 8 are always 1 for CPL when there is no cavity (*i.e.*,  $E_0 = E_{CPL,0}$ ).

## References

1. M. O. Scully, M. S. Zubairy, *Quantum Optics* (Cambridge University Press, 2013).
2. L. D. Barron, *Molecular light scattering and optical activity*, 2nd Ed. (Cambridge University Press, 2009).
3. M. V. Berry, Optical currents. *J. Opt. Pure Appl. Opt.* **11**, 094001 (2009).
4. Y. Tang, A. E. Cohen, Optical chirality and its interaction with matter. *Phys. Rev. Lett.* **104**, 163901 (2010).
5. A. Aiello, M. V. Berry, Note on the helicity decomposition of spin and orbital optical currents. *J. Opt.* **17**, 062001 (2015).
6. K. Y. Bliokh, F. J. Rodríguez-Fortuño, F. Nori, A. V. Zayats, Spin-orbit interactions of light. *Nat. Photonics* **9**, 796–808 (2015).
7. Y. Tang, A. E. Cohen, Enhanced enantioselectivity in excitation of chiral molecules by superchiral light. *Science* **332**, 333–336 (2011).
8. R. M. Kim, *et al.*, Enantioselective sensing by collective circular dichroism. *Nature* **612**, 470–476 (2022).
9. M. L. Solomon, *et al.*, Nanophotonic platforms for chiral sensing and separation. *Acc. Chem. Res.* **53**, 588–598 (2020).
10. X. Zhang, Y. Liu, J. Han, Y. Kivshar, Q. Song, Chiral emission from resonant metasurfaces. *Science* **377**, 1215–1218 (2022).
11. Y. Chen, *et al.*, Observation of intrinsic chiral bound states in the continuum. *Nature* **613**, 474–478 (2023).
12. K. Y. Bliokh, F. Nori, Characterizing optical chirality. *Phys. Rev. A* **83** (2011).
13. S. S. Schweber, *An introduction to relativistic quantum field theory* (Dover Publications, 2005).
14. K. Y. Bliokh, Y. S. Kivshar, F. Nori, Magnetoelectric effects in local light-matter interactions. *Phys. Rev. Lett.* **113**, 033601 (2014).
15. E. Kaxiras, J. D. Joannopoulos, *Quantum Theory of Materials* (Cambridge University Press, 2019).
16. M. L. Cohen, S. G. Louie, *Fundamentals of Condensed Matter Physics* (Cambridge University Press, 2016).
17. M. V. Gorkunov, A. A. Antonov, Y. S. Kivshar, Metasurfaces with maximum chirality empowered by bound states in the continuum. *Phys. Rev. Lett.* **125** (2020).
18. X. Yin, M. Schäferling, B. Metzger, H. Giessen, Interpreting chiral nanophotonic spectra: the plasmonic Born-Kuhn model. *Nano Lett.* **13**, 6238–6243 (2013).

19. D. Englund, *et al.*, Controlling the spontaneous emission rate of single quantum dots in a two-dimensional photonic crystal. *Phys. Rev. Lett.* **95**, 013904 (2005).
20. K. Koshelev, S. Lepeshov, M. Liu, A. Bogdanov, Y. Kivshar, Asymmetric metasurfaces with high- Q resonances governed by bound states in the continuum. *Phys. Rev. Lett.* **121** (2018).

## Figures

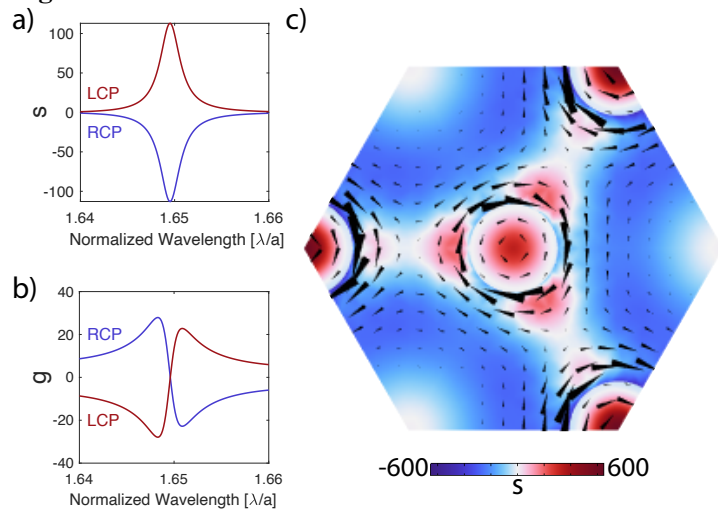


**Figure 1.** Spin dissymmetry of the simulated metasurface, as it is compared to chiral dissymmetry around the q-BIC resonance. a) The spin dissymmetry factor out-of-plane component, showing maximal spin preservation on-resonance. b) The chiral (Kuhn's) dissymmetry factor, showing minimal chirality preservation on-resonance. c) The normalized dissymmetry factor at a plane through the center of the metasurface ( $z = h/2$ ), with arrows indicating the direction of the optical currents (Poynting vectors), taken on-resonance at  $\lambda/a = 1.65$ .

## Tables

**Table 1.** Symmetry comparison of optical cavity enhancement factors.

	P : T Symmetry	Local Density	Enhancement Factor
Purcell Factor	+ : +	$W = \frac{1}{4}( \mathbf{E} ^2 +  \mathbf{H} ^2)$	$f \propto \frac{W_E}{W_{E0}}$
Spin Dissymmetry Factor	+ : -	$\mathbf{S} = \frac{1}{4\omega} \text{Imag}(\mathbf{E}^* \times \mathbf{E} + \mathbf{H}^* \times \mathbf{H})$	$s \propto \frac{S_E}{S_{E0}}$
Kuhn Dissymmetry Factor	- : +	$C = -\frac{1}{2\omega} \text{Imag}(\mathbf{E}^* \cdot \mathbf{H})$	$g \propto \frac{C_{EH}}{C_{EH0}}$

Parity (P) and Time-reversal (T) symmetry transformations are indicated as even (+) or odd (-).

## Supporting Information Text

### I. Poynting vector and wavevector.

We use the same formalism as applied for Equations 3, 4 to arrive at the traditional Poynting vector and inspect its relationship to the local wavevector. By multiplying the energy, spin, and helicity operators simultaneously, we arrive at the Poynting vector,

$$\mathbf{P} = \langle \Psi | \omega \hat{h} \hat{\mathbf{S}} | \Psi \rangle = \frac{1}{2} \text{Real}(\mathbf{E}^* \times \mathbf{H}), \quad (\text{S1})$$

which differs from the local wavevector,

$$\mathbf{k} = \frac{\langle \Psi | \hat{\mathbf{p}} | \Psi \rangle}{|\Psi|^2}. \quad (\text{S2})$$

$\mathbf{P}$  and  $\mathbf{k}$  will point in the same direction in vacuum, but in optical cavities or near material boundaries, the wavevector  $\mathbf{k}$  Equation S1 may be complex, and need not point in the same direction as the power flow  $\mathbf{P}$ . Thus, in free space where the wavevector is real, aligned with the direction of power flow, and homogenous, the chirality and spin of light can be measured as the wavefront polarization transverse to the wavevector direction. Outside of these conditions, local (spatially varying) densities should be defined that are real. Energy density (Eqn 5), chiral density (Eqn 4), and spin density (Eqn 3) can be defined locally without issue, because the final quantities are always real. Traditionally, the relationship between spin and chiral densities are derived by starting with the Poynting vector from Equation S2, which more explicitly shows the relationship between spin and orbital angular momentum rather than between spin and linear momentum (1).

### II. Normalization under Fermi's Golden Rule.

Our spin dissymmetry factor in Equation 6 is closely related to the spin angular momentum of light that is well-known in the literature on the spin-orbit interactions of light (2). We extend the same formalism to the chiral density and electric energy density to emphasize their similarities. Following Fermi's Golden Rule, the normalization of the chiral density (Equation 4) is proportional to the Kuhn dissymmetry factor,

$$g \propto \frac{C}{|\mathbf{E}_0|^2}, \quad (\text{S3})$$

And likewise, the normalization of the electric portion of the electromagnetic energy density (Equation 5) is proportional to the Purcell factor,

$$F_P \propto \frac{W_E}{|\mathbf{E}_0|^2}. \quad (\text{S4})$$

Together, these factors describe Fermi's Golden Rule under three key scenarios: 1. parity-even and time-odd interactions (the spin dissymmetry factor), 2. parity-odd and time-even interactions (Kuhn's dissymmetry factor), and 3. parity-even and time-even interactions (the Purcell factor). The Purcell factor will often take a more detailed form, where the interaction cross-section between the electric field energy density and particle position, their spatial and spectral overlap, as well as nonradiative dissipation mechanisms, are considered. The spin dissymmetry factor can similarly be expanded, but their scaling with respect to the local density of optical states remains intact. In computation, the normalization in the denominator is equivalent to the energy density term in free space, i.e.  $g \propto C/C_{CPL,0}$ .

### III. Optical currents.

In the cited work (1), the Poynting vector lines are referred to more generally as “optical currents,” which we adopt in our description. Such vector contours are useful in description closed surfaces, which is the case in vortices and rotational centers (known as C points). This convention also avoids the confusion of describing local power flow using the Poynting vector, when in fact the wavevector and power flow direction may not co-propagate.

#### **IV. Molecular polarizability.**

Consider the rate of absorption of a particle,  $a = \omega\alpha''|\mathbf{E}|^2$ , where  $\alpha''$  is the imaginary part of the particle polarizability. This solution splits degeneracy when time-reversal symmetry is broken, such that a spin-coupled particle experiences  $A^+$  and  $A^-$  for absorption from left-CPL and right-CPL. The relative absorption of light into a single spin state (i.e., one eigenstate of the Kramers' degenerate pair) is then  $2(a^+ - a^-)/(a^+ + a^-)$ , which is equivalent to Equation 10 (3, 4).

## SI References

1. M. V. Berry, Optical currents. *J. Opt. Pure Appl. Opt.* **11**, 094001 (2009).
2. K. Y. Bliokh, F. J. Rodríguez-Fortuño, F. Nori, A. V. Zayats, Spin–orbit interactions of light. *Nat. Photonics* **9**, 796–808 (2015).
3. Y. Tang, A. E. Cohen, Optical chirality and its interaction with matter. *Phys. Rev. Lett.* **104**, 163901 (2010).
4. L. D. Barron, *Molecular light scattering and optical activity*, 2nd Ed. (Cambridge University Press, 2009).